Astron. Astrophys. 209, 198–210 (1989)

ASTRONOMY
AND
ASTROPHYSICS

A model for a stellar wind driven by linear acoustic waves

F.P. Pijpers[1,2] **and A.G. Hearn**[1]

[1] Sterrewacht Utrecht, Postbus 80000, 3508 TA Utrecht, The Netherlands
[2] Sterrewacht Leiden, Postbus 9513, 2300 RA Leiden, The Netherlands

Received November 30, 1987; accepted May 13, 1988

Summary. A model for a stellar wind driven by acoustic waves in the linear regime is proposed. An equation of transport of momentum is constructed and its topology in the (distance, velocity)-plane investigated. For certain values of the parameters α, expressing the ratio of wave energy flux to thermal energy flux, and λ, the dissipation length of the waves, there are three critical points, one of which is an attractor.

Velocity profiles are calculated for a star of $\mathcal{M} = 16\,\mathcal{M}_\odot$, $R = 400\,R_\odot$, and $T = 10^4$ K. Mass-loss rates ranging from $10^{-28}\,\mathcal{M}_\odot$/yr to $10^{-4}\,\mathcal{M}_\odot$/yr are obtained. Outflow velocities at $150\,R_*$ range from $20\,\mathrm{km\,s^{-1}}$ to $290\,\mathrm{km\,s^{-1}}$.

Key words: hydrodynamics – numerical methods – stars: mass-loss – non-radial pulsations – oscillations

1. Introduction

In 1958 Parker suggested that an extended stellar corona cannot remain static and will drive a mass loss from the star, accelerating it to supersonic velocities. Since that first theory of continuous mass loss, several other mechanisms have been proposed in response to observations of mass loss from stars which apparently do not have a corona.

Linsky and Haisch (1979) found from early observations with the IUE ultraviolet satellite, that late-type stars, which were observed from the circumstellar lines to have a large mass loss, had no transition region and therefore presumably no corona. To explain the mass loss from cool giants Hartmann and MacGregor (1980) proposed a theory of mass loss driven by Alfvén waves. Although the theory can explain the observed mass loss with reasonable fluxes of Alfvén waves, a difficulty has arisen in the final velocity of the wind. The observed final wind velocity is typically half the escape velocity from the surface of the star. The Hartmann and MacGregor theory can reproduce the observed final velocity if the dissipation length of the Alfvén waves is about 1 stellar radius. However Holzer et al. (1983) show that in that case the final wind velocity is extremely sensitive to the dissipation length. This means that the dissipation length would have to agree with the stellar radius to within a few percent for a wide range of stars to reproduce the observed final velocity. This is unlikely. In addition there is no obvious physical mechanism for Alfvén waves that produces such a precisely tuned dissipation length.

The observations of large mass loss from M giants and supergiants with large infrared excesses attributed to dust led to the suggestion that the stellar winds from them may be driven by radiative forces on the dust. Kwok (1975) was the first to calculate a dynamical model for such a wind. The difficulty is that for most of the stars in question the dust apparently can only form at a distance of several stellar radii from the star. Therefore another mechanism is necessary to bring the gas up to a level where the dust can form. Since many of these stars like the Miras undergo radial pulsations, the radial pulsations are the usual choice for a second mechanism for the mass loss. Numerical studies of mass loss driven by radial pulsations were made by Wood (1979) and Willson and Hill (1979) assuming the pulsations are adiabatic or isothermal. More recent calculations by Bowen (1988) including the energy balance within the pulsations more carefully show that radial pulsations without dust cannot drive a significant mass loss. Castor (1987) came to the same conclusion. Mass loss rates in agreement with the observations for Mira stars can be obtained if the dust forms at 2 stellar radii. Whether or not the dust can form at so close to the star remains an unanswered question.

As an alternative approach to these problems, a theory of mass loss driven by sound waves is developed in the present paper. The idea of a stellar wind driven by sound waves was rejected by Hartmann and MacGregor (1980) on the grounds that in a hydrostatic stellar atmosphere the dissipation length is comparable to the photospheric density scale height, which is a few percent of a stellar radius for late-type stars. In a stellar wind the density scale height is about one stellar radius. The dissipation length of the waves scales with the density scale height and, as the present paper shows, waves with a dissipation length of one stellar radius can effectively drive a stellar wind. Sound wave driven wind models are calculated here for a star of $16\,\mathcal{M}_\odot$ and $400\,R_\odot$ with a wind temperature of 10,000 K. These are the same parameters as the first six cases given by Hartmann and MacGregor (1980) for their theory of Alfven wave driven winds. A stellar wind driven by sound waves has a much lower final velocity than a wind driven by Alfvén waves. This is explained by the Alfvén speed being much higher than the sound speed in the stellar wind models in question. The final velocity of the sound wave driven wind is not sensitive to the dissipation length as it is for Alfvén wave driven winds.

Send offprint request to: F.P. Pijpers (Utrecht)

2. The model

To describe the gasflow in a stellar wind the full equations of the transport of mass, momentum and energy must be solved. A general solution to these equations without any restrictions is difficult. In this paper a model of a stellar wind driven by sound waves of short wavelength is described. To simplify the calculation the following assumptions have been made.

1) The flow is stationary.
2) The wind is spherically symmetric.
3) The direction of the flow and the wavevectors is purely radial.
4) The wavelength of the waves is shorter than the typical pressure and density scale heights of the wind.
5) The matter in the wind is a perfect gas of homogeneous composition.
6) Viscosity is neglected.
7) Either purely adiabatic or purely isothermal waves are used.
8) Neither the formation nor the presence of dust in the flow is considered, which implies that radiation pressure on the dust is neglected.
9) The contribution of radiation pressure to the forces acting on the gas is neglected. This restricts applications of this model to spectral types later than approximately type B5.
10) The atmosphere is isothermal.

With these assumptions the equation of transport of mass becomes:

$$\frac{d}{dr}(\rho u r^2) = 0 \tag{1}$$

This can immediately be integrated, which yields:

$$\rho u r^2 = \rho_0 u_0 r_0^2 = \dot{\mathcal{M}}/4\pi \tag{2}$$

The sign convention of a positive sign of $\dot{\mathcal{M}}$ for mass-*loss* will be used. u is the velocity of the local mean flow of the gas at position r. ρ is the gas density. The subscript zero refers to the value of the variable at an arbitrary reference level $r = r_0$.
The equation of motion is:

$$\rho u\left(\frac{du}{dr}\right) = -\frac{dp}{dr} - (\nabla \cdot \mathbf{P}_{\mathrm{w}})_r + \rho g \tag{3}$$

Where $\mathbf{P}_{\mathrm{w}}$ is the pressure tensor resulting from the waves and p is the gas pressure which is related to the density through the equation of state, which for a perfect gas is:

$$p = \rho \frac{kT}{\mu m} \tag{4}$$

where k is Boltzmann's constant, μ the average molecular weight, m is the atomic mass unit, and T the local gas temperature. g is the local acceleration of a gas element due to gravity:

$$g = -\frac{G\mathcal{M}}{r^2} \tag{5}$$

where G is the gravitational constant and $\mathcal{M}$ is the mass of the star. Since acoustic waves are present in the wind, a term $\mathbf{P}_{\mathrm{w}}$ appears in equation (3). $\mathbf{P}_{\mathrm{w}}$ is the pressure tensor that arises from the selfinteraction, averaged in time over a wave period, of the acoustic waves. Only the radial component of the divergence of this tensor appears in Eq. (3) because of the assumption of spherically symmetric flow. Pressure has in general the character of a tensor (Landau and Lifshitz, 1959). Only in an isotropic medium without velocity gradients, such as a perfect gas undisturbed by waves, will this tensor reduce to a scalar. In Eq. (3) this scalar part, the normal gas pressure p, has been separated from the rest of $\mathbf{P}_{\mathrm{w}}$ which for sound waves then takes the form:

$$\mathbf{P}_{\mathrm{w}_{ij}} = E\left(\frac{\kappa_i \kappa_j}{|\kappa|^2} + \frac{\rho}{a}\frac{\partial a}{\partial \rho}\delta_{ij}\right) \qquad i, j = r, \theta \text{ and } \phi \tag{6}$$

E is the energy-density of the acoustic waves:

$$E = \tfrac{1}{2}\rho\langle \delta u^2 \rangle \tag{7}$$

where $\langle \delta u^2 \rangle$ is the mean of the velocity amplitude squared of the wave, κ is the wave vector of the acoustic waves. The sound speed a is defined by:

$$a^2 = b_0 \frac{kT}{\mu m} \tag{8}$$

The constant b_0 equals 1 for isothermal waves and γ for adiabatic waves, where γ is the ratio of specific heats. Under the restrictions listed above, equation (6) reduces to:

$$P_{\mathrm{w}} = \begin{pmatrix} b_1 E & 0 & 0 \\ 0 & b_2 E & 0 \\ 0 & 0 & b_2 E \end{pmatrix} \tag{9a}$$

The constants b_0, b_1 and b_2 are:

Wavetype	Adiabatic	Isothermal
b_0	γ	1
b_1	$\frac{1}{2}(\gamma + 1)$	1
b_2	$\frac{1}{2}(\gamma - 1)$	0

(9b)

Equation (6), derived by Bretherton (1970), is strictly valid only for sinusoidal wavetrains, propagating in a slowly varying medium. Equation (9a) will be used in this paper, which means that the equations are applicable only to monochromatic waves with wavelengths shorter than the typical pressure and density scale heights of the gas.

Even in the absence of dissipation of the waves, their energy density E is not a conserved quantity of the flow, because of the interaction of the wave with the accelerating gas in the stellar wind. The wave action density is conserved (Bretherton, 1970). This is defined by:

$$A \equiv E/(\omega - u\kappa) \tag{10}$$

Therefore:

$$\frac{\partial A}{\partial t} + \nabla \cdot (V_{\mathrm{w}} A) = 0 \tag{11}$$

V_{w} is the wave group velocity which equals $u + a$. Dissipation of first order in A will be included (Bretherton, 1970; Jacques, 1977):

$$\frac{\partial A}{\partial t} + \nabla \cdot (V_{\mathrm{w}} A) = -\frac{V_{\mathrm{w}} A}{L} \tag{12}$$

The dissipation length L is assumed to be constant throughout the atmosphere, following the analysis of Hartmann and MacGregor (1980) for Alfvén wave driven winds. In general sound waves will rapidly steepen to form shocks and this will determine the dissipation of the waves. The dissipation length is a function of the amplitude of the waves and is not constant throughout the atmosphere. For this linearised analysis, the dissipation length is assumed to be constant for simplicity, and a specified value so that the sensitivity of the solution to the dissipation length can be seen. The assumption of an isothermal mean atmosphere removes the coupling between the dissipation of the waves and the temperature of the atmosphere. In steady state and for spherical symmetry equation (12) can easily be integrated, giving:

$$V_w A r^2 = (V_w A r^2)_0 \exp[(r_0 - r)/L] \tag{13}$$

The subscript zero again refers to values at the reference level $r = r_0 \cdot E$ can be substituted back into Eq. (13), which becomes:

$$\frac{V_w E r^2}{\omega - u\kappa} = \text{constant} \exp[(r_0 - r)/L] \tag{14}$$

It is well known from geometrical acoustics that ω is a constant (Landau and Lifshitz, 1959). After multiplication of Eq. (14) by ω, the constant on the right-hand side therefore remains constant. Making use of the dispersion relation for sound waves:

$$\omega = (u + a)\kappa \tag{15}$$

yields the expression for E:

$$E = E_0 \frac{(u_0 + a)^2}{(u + a)^2} \frac{r_0^2}{r^2} \exp[(r_0 - r)/L] \quad \text{for } r \geqq r_0 \tag{16}$$

Equation (12) loses its validity at some radius within the star where the waves are generated, because source terms would then have to be included. To avoid this problem, Eq. (12) and following are assumed only to be valid outside the photospheric radius r_0. By substituting Eq. (9a) the term $\nabla \cdot \mathbf{P}_w$ in Eq. (3) reduces to:

$$(\nabla \cdot \mathbf{P}_w)_r = b_1 \frac{dE}{dr} + \frac{2E}{r} \qquad (\nabla \cdot \mathbf{P}_w)_\theta = (\nabla \cdot \mathbf{P}_w)_\phi = 0 \tag{17}$$

For numerical purposes the following dimensionless variables are used:

$$\begin{aligned} \xi &= r/r_0 \\ M &= u/a \\ \varepsilon &= E/(\tfrac{3}{2}p) \end{aligned} \tag{18}$$

where ξ is a dimensionless distance, M is the Mach number and ε is a dimensionless energy density. With Eqs. (2) and (16) an expression for ε is obtained:

$$\varepsilon = \alpha \frac{M}{(M+1)^2} \exp[(1 - \xi)/\lambda] \quad \text{for } \xi \geqq 1 \tag{19}$$

where λ is L/r_0. α is defined by:

$$\alpha = \frac{2}{3} b_0 \frac{(M_0 + 1)^2}{\rho_0 M_0 a^2} E_0 \tag{20}$$

α is related to the mechanical flux and thermal flux as follows. The mechanical flux F_m of the sound waves is defined by:

$$F_m = V_w E + u{:}\mathbf{P} = [(b_1 + 1)M + 1]aE \tag{21a}$$

The mechanical flux of the sound waves at the stellar surface then is:

$$F_m(r = r_0) = [(b_1 + 1)M_0 + 1]aE_0 \tag{21b}$$

The thermal flux F_{th}, i.e. the flux of internal energy of the gas advected by the fluid motion, is defined by:

$$F_{th} = \rho u \frac{3kT}{2\mu m} = \rho u \frac{3a^2}{2b_0} \tag{22a}$$

At the stellar surface $F_{th}(r = r_0)$ is:

$$F_{th}(r = r_0) = \frac{3\rho_0 M_0 a^3}{2b_0} = \frac{\dot{\mathcal{M}}}{4\pi r_0^2} \frac{3a^2}{2b_0} \tag{22b}$$

Because T, and therefore a, is assumed to be constant throughout the atmosphere, the thermal luminosity $r^2 F_{th}$ is conserved. Substituting Eqs. (21b) and (22b) in Eq. (20) yields:

$$\alpha = \frac{(M_0 + 1)^2}{(b_1 + 1)M_0 + 1} \frac{F_m(r = r_0)}{F_{th}(r = r_0)} \tag{23}$$

For low Mach numbers $M_0 \ll 1$:

$$\alpha = \frac{F_m(r = r_0)}{F_{th}(r = r_0)} \tag{24}$$

In addition the dimensionless variable Ψ is used.

$$\Psi = \frac{b_0}{2} \frac{G\mathcal{M}}{a^2 r_0} = \frac{r_p}{r_0} = \frac{3F_{gr}(r = r_0)}{4F_{th}(r = r_0)} \tag{25}$$

r_p is the distance of the critical point in the Parker theory. Ψ is the ratio of the gravitational energy flux at the stellar surface to the thermal energy flux at the stellar surface, multiplied by $\frac{3}{4}$. The gravitational energy flux is defined by:

$$F_{gr} = \rho u \frac{G\mathcal{M}}{r} \tag{26a}$$

and therefore at the stellar surface:

$$F_{gr} = \rho_0 u_0 \frac{G\mathcal{M}}{r_0} = \rho_0 u_0 \frac{v_e^2}{2} \tag{26b}$$

where v_e is the escape velocity at the stellar surface.

With these new variables and the substitution of Eq. (2), Eq. (3) becomes:

$$\begin{aligned} \frac{1}{M}\frac{dM}{d\xi}\left(1 + \frac{3b_1 M\varepsilon}{M+1} - b_0 M^2\right) &= \frac{2\Psi}{\xi^2} + \frac{1}{2T}\left(1 - \frac{3}{2}b_1\varepsilon + b_0 M^2\right)\cdot\frac{dT}{d\xi} \\ &\quad - \frac{2}{\xi}\left(1 + \frac{3}{2}b_2\varepsilon\right) - \frac{3b_1\varepsilon}{2\lambda} \end{aligned} \tag{27}$$

As the atmosphere is assumed to be isothermal the second term on the righthand side of Eq. (27) disappears and the equation of motion becomes:

$$\frac{1}{M}\frac{dM}{d\xi}\left(1 + \frac{3b_1 M\varepsilon}{M+1} - b_0 M^2\right) = \frac{2\Psi}{\xi^2} - \frac{2}{\xi}\left(1 + \frac{3}{2}b_2\varepsilon\right) - \frac{3b_1\varepsilon}{2\lambda} \tag{28}$$

From Eqs. (19) and (28), it can be seen that the model is fully determined by four parameters:

- b_0, or the choice of wavetype; which determines b_0, b_1 and b_2.
- λ; the dissipation length of the waves in stellar radii.
- α; the ratio of wave energy flux to thermal energy flux.
- Ψ; the ratio of gravitational to thermal energy-density.

Ψ is specified by the stellar mass and radius and the temperature of the wind. For solar units and degrees Kelvin:

$$\Psi = 1.15\,10^7\,\mu \frac{\mathcal{M}}{r_0 T} \tag{29}$$

Given the choice of the sound wave and its dissipation length, the main parameter of the calculation is α. The solution of Eq. (28) gives the velocity of the wind as a function of distance from the centre of the star. The solution is unique except for some cases where there are three critical points and sometimes two valid solutions.

α is not a directly observable parameter. Equation (23) shows that it is related to the ratio of the mechanical flux of the sound waves at the base of the wind to the thermal flux of internal energy advected by the wind. Equations (7) and (20) combined give:

$$\alpha = \frac{b_0}{3a^2} \frac{(M_0+1)^2}{M_0} \langle \delta u^2 \rangle_0 \tag{30}$$

which shows that the parameter α specifies the mean velocity amplitude squared of the sound waves at the base of the wind. The Mach number M_0 at the base of the wind changes very rapidly with α, so that the relationship between α and $\langle \delta u^2 \rangle_0$ in equation (30) is a very non-linear one.

To convert the solution to physical parameters the density ρ_0 at the base of the wind must be specified. The density does not appear in Eq. (28), which is usual in stellar wind equations obtained by combining the equations of motion and continuity. For a given assumed density, Eq. (21b) gives the mechanical flux of sound waves at the base of the wind which is driving the wind and Eq. (2) gives the total mass loss rate of the wind. Both these equations depend once again on the velocity at the base of the wind obtained from the solution of Eq. (28).

Satisfying double boundary conditions involves shooting methods. Parker (1958) showed that the only solution that is subsonic at the stellar surface and supersonic at infinity passes through the critical point. Equation (28) is therefore integrated from the critical point. This implies that the purely subsonic breeze solutions will not be considered.

3. Method of solution

3.1. General properties of critical points

Inherent in theories of stationary stellar winds is the existence of one or more critical points. At such a critical point both lefthand and righthand sides of the equation of motion Eq. (28), become zero. The critical points are important for the construction of the supersonic solutions because only these points are known a priori to lie on this solution. Equation (28) is then integrated inward from the critical point towards the stellar surface and outward to a large but finite distance.

To integrate Eq. (28), not only the values of ξ and M are required at the critical point, but also $\frac{dM}{d\xi}$. These initial values are discussed in Appendix A. Because Eq. (28) is singular at the critical point $\left(\frac{dM}{d\xi}\right)_c$ must be obtained by using l'Hospitals rule (Abramowitz and Stegun, 1970). It can also be found by constructing a first-order Taylor expansion around the critical point, which is somewhat less straightforward. This procedure is treated in Appendix B. The advantage of this procedure is that if the critical point is an attractor, it will be readily identified as such.

Velocity curves passing near an attractor will try to spiral into it. In a continuous stellar wind the velocity profiles have to be single valued in M for all ξ. Solutions spiralling near an attractor are not single valued and therefore not physically valid. No continuous, physically valid solution to Eq. (28) can be constructed near such points. An investigation of the equation of motion in Appendix A shows that for certain ranges of values of the parameters α and λ three critical points exist. Critical point number 2 (Figs. 1c, 1d) turns out always to be an attractor. This generally does not affect the wind solutions passing through the other critical points. In most of these cases two wind solutions exist but in some cases only the solution passing through the critical point furthest away from the attractor remains.

For a given star, which defines Ψ, and a given dissipation length λ, solutions are calculated for a range of values of α. The integration from the critical point is done with a fourth-order Adams predictor-corrector method (Hall and Watt, 1976). The integration outward is extended to 150 stellar radii. For some solutions the integration towards the stellar surface gives a Mach number M which decreases very rapidly to small values. In such cases the numerical integration may not be sufficiently accurate. An analytical solution to Eq. (28) is then used which is correct to first order near the stellar surface. Similarly the solution may be extrapolated to infinity using an analytical solution.

3.2. Analytical solution near the stellar surface

All terms in Eq. (28) can be expanded to first order in ξ and M around the point $(\xi, \mathrm{M}) = (1, 0)$. With new variables defined by:

$$\begin{aligned} x &= \xi - 1 \\ y &= M \end{aligned} \tag{31}$$

Eq. (28) reduces to the form:

$$\frac{1}{y}\frac{dy}{dx} = A - Bx - Cy \qquad x, y \ll 1 \tag{31}$$

where A, B, and C are constants:

$$\begin{aligned} A &= 2\Psi - 2 \\ B &= 4\Psi - 2 \\ C &= 3b_2\alpha + \frac{3b_1\alpha}{2\lambda} \end{aligned} \tag{33}$$

This is a nonlinear form of Bernouilli's equation and can be immediately integrated to give:

$$\begin{aligned} &\frac{1}{y}\exp\left[Ax - \tfrac{1}{2}Bx^2\right] \\ &\quad = C\sqrt{\left(\frac{2\pi}{B}\right)}\exp\left[\frac{A^2}{2B}\right] \\ &\qquad \left[P\left(\frac{A}{\sqrt{B}}\right) - P\left(\left(\frac{A}{B} - x\right)\sqrt{B}\right)\right] + \frac{1}{y_0} \end{aligned} \tag{34}$$

where

$$P(t) = \frac{1}{\sqrt{(2\pi)}} \int_{-\infty}^{t} \exp\left[-\tfrac{1}{2}t'^2\right] dt' \tag{35}$$

The numerical solution of Eq. (28) can be extrapolated to the stellar surface using Eq. (34) with a suitable value of the constant y_0. The term containing the constant C is usually very small. Equation (34) then reduces to a simple law of exponential growth for y.

3.3. Analytical solution at infinity

For very large distances, ε drops exponentially to zero for finite λ. Equation (28) can be approximated by the following analytically integrable differential equation:

$$\frac{1}{M}(1 - b_0 M^2)\frac{dM}{d\xi} = \frac{2\Psi}{\xi^2} - \frac{2}{\xi} \tag{36}$$

This is the equation of motion of the Parker theory (1958). Integration yields:

$$\log M - \tfrac{1}{2} b_0 M^2 = -\frac{2\Psi}{\xi} - 2\log\xi + \text{const.} \tag{37}$$

The numerical solution of Eq. (28) can be extrapolated to infinity using Eq. (37) with a suitable value of the constant.

4. The critical points

An analysis of the lefthand and righthand sides of Eq. (28) shows that if the dissipation length λ is larger than a certain threshold value the topology of the equations is simple with only one critical point. The topology of the equations in this case is depicted in Fig. 1a and is independent of the parameter α. If the dissipation length λ is less than that threshold value the topology becomes much more complicated with the possibility of multiple critical points if α is in the right range. Figures 1a to 1e show the progression of the solutions of the lefthand and righthand sides of (28), plotted as curves I and II respectively. α is increasing from Figs. 1a to 1e and λ is less than the threshold value. On curve I the lefthand side of Eq. (28) is zero and on curves II the righthand side is zero. The intersections of curves I and II are the critical points. The plus and minus signs give the sign of $\frac{dM}{d\xi}$ for the areas bounded by the curves I and II and the axes. The scale on the vertical axis of the figures has been omitted because the point of intersection of curve I with the vertical axis cannot be determined analytically. Figures 1a to 1e are in this respect slightly misleading because this point of intersection rises for increasing α. This is suppressed in the figures to show the structure of curve II. Note that in Figs. 1b and 1c, curve II is split in 2 isolated branches labelled II^a and II^b, whereas in figures 1d and 1e these two branches have merged into curve $\mathrm{II}^{a,b}$.

As α increases, that is as the wave energy flux increases, critical point number 1 will move inward and upward and critical point number 2 will move downward and outward. The third critical point will behave like the first. This happens because the region enclosed by II^b expands as α increases.

Curve I determines the velocity at the critical point. In the Parker theory, curve I is a horizontal line at M equal to $1/\sqrt{b_0}$, which is drawn as a dash dotted line. If waves are present the velocity at the critical point will be higher if the critical point is nearer to the stellar surface. This is because the energy density of the waves is not only a function of ξ but also of M since the waves experience a Doppler shift in the flow. This dependence on M causes the presence of the second term on the lefthand side of (28) and therefore the shape of curve I. It is obvious that the critical point must lie closer to the star than the critical point of the Parker theory, that is to the left of the vertical dash dotted line at $\xi = \Psi$, because the acceleration of the gas by the waves is greater. These constraints for ξ_c and M_c are derived in Appendix A.

If the dissipation length λ is larger than the threshold value, which is approximately 5 in the present case, curve II^b will not be formed for any value of α. Critical points 2 and 3 will then also be nonexistent. This can be understood from the physical meaning of the righthand side of Eq. (28). The various terms represent the gravitational, thermal and mechanical contributions to the energy of the gas. If the dissipation length is larger than the threshold value, the second term on the righthand side of Eq. (28) is greater than the third and the waves will transfer just enough momentum to the gas to dominate the momentum balance of the wind at all ξ. This means that the wind will always accelerate.

For very short dissipation lengths λ, the third term in the lefthand side of Eq. (28) is greater than the second. This means that the waves transfer most of their energy and momentum to the gas very near to the stellar surface, which causes a rapid acceleration of the gas. At slightly larger distances from the stellar surface so much energy has already been dissipated that the gravitational pull on the gas again starts to dominate. This is the region enclosed by curve II^b. Because there is an extra critical point (see Figs. 1c and 1d) the gas can pass curve I very near the star. When this gas leaves the region enclosed by curve II^b it will decelerate for a short distance up to $\xi \simeq \Psi$ where it crosses curve IIa. The total thermal and mechanical energy is large enough to let the matter escape the star. All mechanical energy will be converted into thermal energy so that eventually the gas will accelerate again in a Parker-like solution toward infinity, given by Eq. (37).

Note that for those dissipation lengths for which there are three critical points, the solution of Eq. (28) passing through critical point 1 conforms closely to the classical Parker solution and will be referred to as the 'low velocity' solution. The solution passing through critical point 3 will have a higher velocity than this 'low velocity' solution throughout the wind, and will therefore be referred to as the 'high velocity' solution.

If λ is larger than the threshold value, there is only one solution, which will be referred to as the 'high velocity' solution as well. No continuous solution passes through critical point 2.

5. The results

Models of winds driven by adiabatic and isothermal sound waves have been calculated for an isothermal atmosphere of a star of $16\,\mathcal{M}_\odot$ and $400\,R_\odot$. The electron temperature of the wind is 10^4 K and the mean atomic weight $\mu = 0.667$. This is identical to the first six models calculated by Hartmann and MacGregor (1980) for Alfvén wave driven winds. The value of the parameter Ψ for such a star is 30.77 and the escape velocity at the stellar surface is $123.5\,\mathrm{km\,s^{-1}}$. The isothermal sound speed is $11.13\,\mathrm{km\,s^{-1}}$ and the adiabatic sound speed is $14.37\,\mathrm{km\,s^{-1}}$, where γ is $\frac{5}{3}$.

Table 1 gives the velocity of the wind at 150 stellar radii driven by adiabatic and isothermal waves, calculated for a range

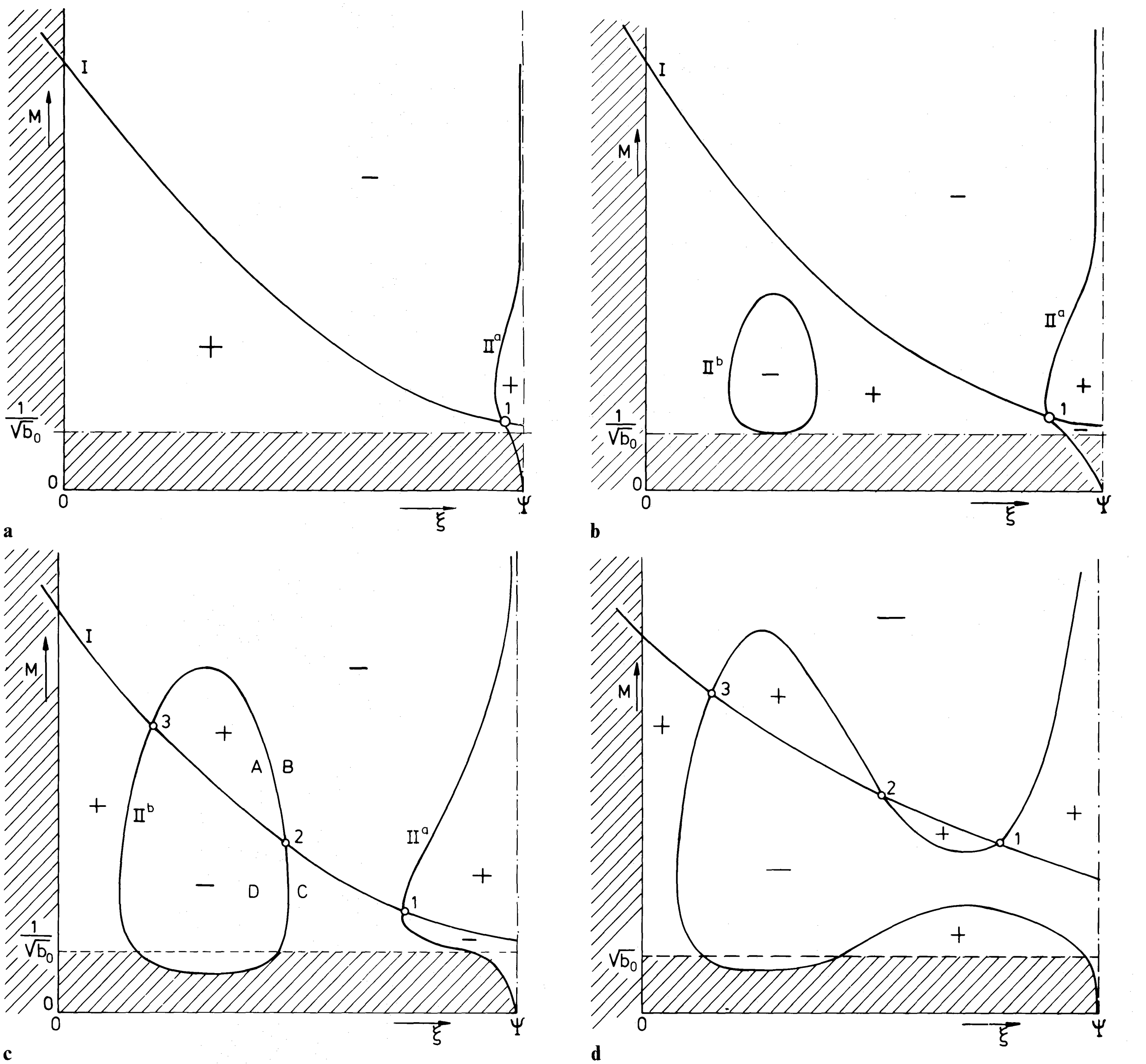

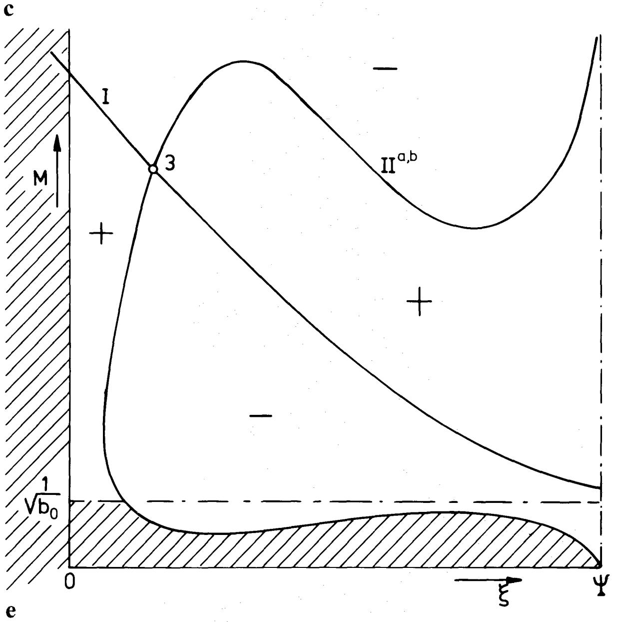

Fig. 1a–e. Topology of the equation of motion. α increasing from **a** to **e**. $\pm$ = sign of $dM/d\xi$. o = critical points. At curve I $dM/d\xi = \pm\infty$, at curve II $dM/d\xi = 0$

of λ, the dissipation length of the waves in stellar radii, and α, which is related to the ratio of the mechanical energy flux to the thermal energy flux by Eq. (24). Table 2 gives the velocity of the wind at the stellar surface. Table 3 gives the velocity of the wind at the critical point. Table 4 gives the distance of the critical point in stellar radii. Tables 1, 2, 3 and 4 all give values for high velocity solutions. For those values of α and λ for which three critical points are found the low velocity solutions are described in the notes to the tables.

Note that, as in the Parker wind equation, the density has been eliminated from the equation of motion by combining it with the equation of continuity. This implies that the density profile is determined by the velocity profile. The density at some point in the wind, e.g. at the stellar surface, must be specified to obtain a full wind solution.

In several cases the critical point was found but no velocity profile was calculated because either the critical point was situated below the stellar surface or the low velocity solution spiralled into the attractor.

5.1. *The wind at 150 stellar radii*

Tables 1 and 3 show that the velocity of the wind at 150 stellar radii and at the critical point vary little for a wide range of values of α and λ. In most cases is the wind velocity at 150 stellar radii less than the escape velocity at the stellar surface. This is illustrated in Fig. 2 where the outflow velocity of the wind at 150 stellar radii is plotted against the dissipation length λ, for various values of α. The results for adiabatic sound waves are shown. The parts of the curves drawn as dashed lines are the high velocity solutions. In these cases there is also a low velocity solution which coincides with the solid line for α equal to zero. The outflow velocity at the critical point is plotted in Fig. 3. Isothermal waves give a very similar result and are not shown in a figure.

From Tables 1a and 1b it can be seen that adiabatic waves drive a wind with a slightly higher velocity at 150 stellar radii than isothermal waves do, for identical values of the parameters. This can be immediately understood from the fact that the wave pressure gradient arising from the adiabatic waves is slightly greater.

A more remarkable result is that for dissipationless isothermal waves with large α the outflow velocity at 150 stellar radii is lower than for λ equal to 10 for the same value of α. This behaviour is not seen for adiabatic waves. It is explained by the fact that for nondissipative isothermal waves the critical point is

Table 1. Velocity of the wind in km s^{-1} at 150 stellar radii

Adiabatic waves

α \ λ	1	2	5	10	∞
0	27.12	27.12	27.12	27.12	27.12
10	27.12	27.12	27.19	29.86	49.49
20	27.12	27.12	27.26	38.45	63.14
50	27.12	27.12	46.03	63.17	89.42
100	27.12	40.02[c]	75.04	90.53	117.2
200	68.79[c]	89.12[c]	112.4	126.6	153.6
500	[a c]	[a b]	178.6	191.4	219.1
1000	[a c]	[a b]	[a]	[a]	285.7

Isothermal waves

α \ λ	1	2	5	10	∞
0	27.12	27.12	27.12	27.12	27.12
10	27.12	27.12	27.17	28.44	37.13
20	27.12	27.12	27.21	31.59	43.38
50	27.12	27.12	29.32	45.22	55.45
100	27.12	27.12	48.39	63.03	68.05
200	27.12	44.23[c]	74.30	87.25	84.35
500	92.46[c]	102.6[c]	120.2	130.8	113.1
1000	[a c]	155.4[b]	165.8	174.5	141.7

[a] The critical point is situated below the stellar surface where (11) is invalid.
[b] Low-velocity solution spirals into critical point number 2.
[c] A low-velocity solution exists with a wind velocity at 150 stellar radii of 27.12 km s^{-1}.

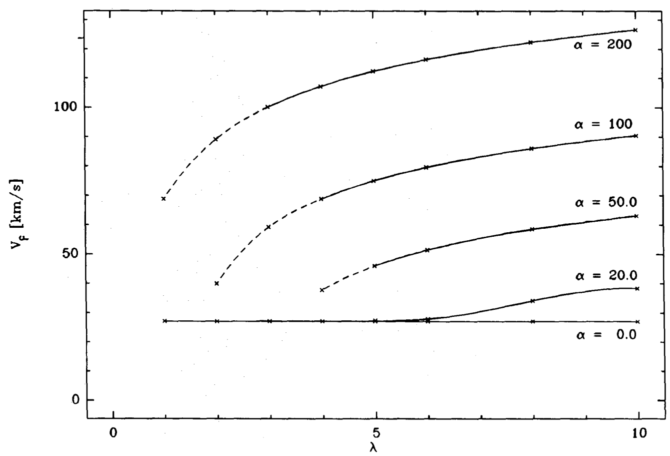

Fig. 2. Velocity at $150r_0$ as a function of λ for various values of α. Dashed parts of the curves correspond to high velocity solutions. Low velocity solutions for the same values of α and λ coincide with the solid curve for $\alpha = 0.0$

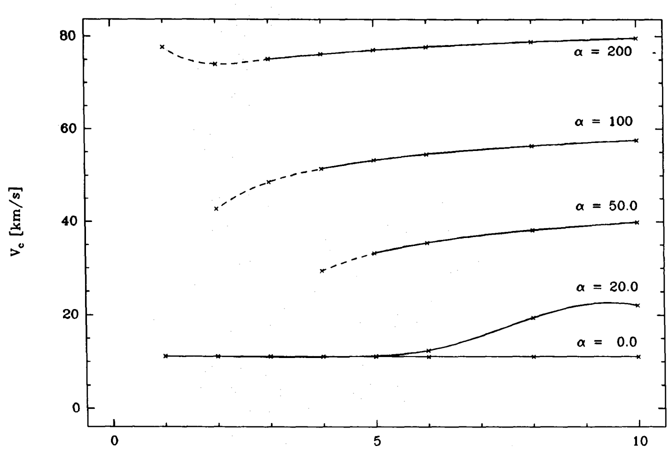

Fig. 3. Velocity at the critical point as a function of λ for various values of α. Dashed parts of curves are high-velocity solutions. Corresponding low-velocity solutions coincide with the solid curve for $\alpha = 0.0$

Table 2. Velocity of the wind in km/s at the stellar surface

Adiabatic waves

α \ λ	1	2	5	10	∞
0	$8.848\,10^{-23}$	$8.848\,10^{-23}$	$8.848\,10^{-23}$	$8.848\,10^{-23}$	$8.848\,10^{-23}$
10	$8.862\,10^{-23}$	$9.207\,10^{-23}$	$1.786\,10^{-22}$	$2.571\,10^{-21}$	$6.994\,10^{-20}$
20	$8.876\,10^{-23}$	$9.596\,10^{-23}$	$8.234\,10^{-22}$	$2.022\,10^{-17}$	$9.001\,10^{-16}$
50	$8.918\,10^{-23}$	$1.093\,10^{-22}$	$2.036\,10^{-2}$	$1.956\,10^{-1}$	$3.499\,10^{-1}$
100	$8.990\,10^{-23}$	25.26[c]	24.43	23.62	22.50
200	73.93[c]	60.50[c]	53.64	51.27	48.64
500	[a c]	[a b]	107.6	102.6	97.27
1000	[a c]	[a b]	[a]	[a]	148.3

Isothermal waves

α \ λ	1	2	5	10	∞
0	$8.848\,10^{-23}$	$8.848\,10^{-23}$	$8.848\,10^{-23}$	$8.848\,10^{-23}$	$8.848\,10^{-23}$
10	$8.861\,10^{-23}$	$9.154\,10^{-23}$	$1.485\,10^{-22}$	$5.754\,10^{-22}$	$3.362\,10^{-21}$
20	$8.873\,10^{-23}$	$9.484\,10^{-23}$	$3.405\,10^{-22}$	$3.596\,10^{-20}$	$4.382\,10^{-19}$
50	$8.911\,10^{-23}$	$1.062\,10^{-22}$	$2.553\,10^{-14}$	$1.421\,10^{-11}$	$1.654\,10^{-11}$
100	$8.974\,10^{-23}$	$1.323\,10^{-22}$	5.932	5.799	3.985
200	$9.104\,10^{-23}$	27.10[c]	24.35	22.69	18.89
500	86.27[c]	68.29[d]	57.65	53.25	44.76
1000	[a c]	110.6[b]	95.51	85.19	71.53

[a] The critical point was situated below the stellar surface where (11) is invalid.
[b] Low velocity solutions spiral into critical point number 2.
[c] A low velocity solution exists with a wind velocity at the stellar surface of the order of $10\,10^{-23}$ km s^{-1}.
[d] The low velocity solution has a wind velocity at the stellar surface of 32.61 km s^{-1}.

Table 3. Velocity of the wind in km s^{-1} at the critical point

Adiabatic waves

α \ λ	1	2	5	10	∞
0	11.13	11.13	11.13	11.13	11.13
10	11.13	11.13	11.18	14.04	24.69
20	11.13	11.13	11.27	22.13	33.11
50	11.13	11.13	33.24	39.91	48.67
100	11.13	42.71[b]	53.27	57.58	64.44
200	77.67[b]	74.05[b]	77.07	79.64	84.50
500	[a b]	[a b]	117.0	117.4	119.4
1000	[a b]	[a b]	[a]	[a]	154.0

Isothermal waves

α \ λ	1	2	5	10	∞
0	11.13	11.13	11.13	11.13	11.13
10	11.13	11.13	11.17	12.58	22.16
20	11.13	11.13	11.23	16.45	29.00
50	11.13	11.13	18.11	29.04	41.82
100	11.13	11.13	36.29	42.79	54.87
200	11.13	45.40[b]	55.63	60.30	71.54
500	91.56[b]	85.61[b]	87.83	90.65	100.6
1000	[a b]	121.5[b]	119.2	120.6	129.4

[a] The critical point is situated below the stellar surface.
[b] A low velocity solution exists with a wind velocity at the critical point of 11.13 km s^{-1}.

Table 4. Distance of the critical point in stellar radii

Adiabatic waves

α \ λ	1	2	5	10	∞
0	30.77	30.77	30.77	30.77	30.77
10	30.77	30.77	29.77	18.17	17.33
20	30.77	30.77	28.35	10.61	12.78
50	30.77	30.77	5.539	5.765	7.823
100	30.77	3.016[b]	3.361	3.804	5.154
200	1.218[b]	1.681[b]	2.189	2.531	3.316
500	[a b]	[a b]	1.272	1.466	1.812
1000	[a b]	[a b]	[a]	[a]	1.139

Isothermal waves

α \ λ	1	2	5	10	∞
0	30.77	30.77	30.77	30.77	30.77
10	30.77	30.77	30.10	23.52	30.77
20	30.77	30.77	29.27	16.79	30.77
50	30.77	30.77	11.91	10.14	30.77
100	30.77	30.77	6.243	7.349	30.77
200	30.77	3.356[b]	4.289	5.489	30.77
500	1.256[b]	1.875[b]	2.844	3.833	30.77
1000	[a b]	1.351[b]	2.147	2.958	30.77

[a] The critical point is situated below the stellar surface.
[b] A low velocity solution exists with a distance of the critical point of 30.77 stellar radii.

always at $\xi = \Psi$, equal to 30.77, instead of moving inward for increasing α (see Appendix A). Therefore the wind reaches its final velocity at greater distances.

These results show one of the main differences between the sound-wave-driven winds and Alfén-wave-driven winds. The winds driven by Alfvén waves with no dissipation have a final velocity which is several times the escape velocity fom the surface of the star, whereas most of the sound wave driven winds have a final velocity well below the escape velocity from the surface of the star.

5.2. *The velocity at the stellar surface*

Table 2 gives the velocity of the wind at the photosphere for a range of values for α and λ. In contrast to the wind velocity at 150 stellar radii, it depends very strongly on α and λ, rising by 24 orders of magnitude within the table. This means that the mass loss rate is also strongly dependent on α and λ. By combining Eqs. (23) and (24) an expression for the mass loss rate as a function of the mechanical flux and α is obtained.

$$\dot{\mathscr{M}} = \frac{8\pi r_0^2}{3a^2} b_0 \frac{(M_0+1)^2}{(b_1+1)M_0+1} \frac{F_{\mathrm{m}}(r=r_0)}{\alpha} \tag{38}$$

The mass loss rate is seen to be a linear function of mechanical flux and only weakly dependent on M_0 for $M_0 \ll 1$, which implies a weak dependence on α and λ. This means that the mass loss rate and mechanical flux behave equally non-linear as functions of α and λ.

Equation (38) is a consequence of Eqs. (2), (20) and (21a), which show that for a solution for a given value of α and λ the mechanical flux of sound waves driving the wind and the calculated mass loss rate are both linearly dependent on the density ρ_0 assumed for the base of the wind.

5.3. *Velocity profiles of the wind*

Figure 4 shows the velocity of the wind plotted against distance in stellar radii for α of 100 and λ of 10. The decelerating solution through the critical point is also shown. This velocity profile is typical of solutions for large α and for which the dissipation length λ is higher than $\lambda_{\mathrm{crit.}}$ below which three critical points are found. The critical point is near the stellar surface and the solutions yield relatively high speed winds (relative to the sound speed) and a high mass loss rate.

Figure 5 shows the velocity of the wind plotted against distance in stellar radii for α equal to 100 and λ equal to 2. This solution has 3 critical points, two of which have real velocity gradients. The lower solid line curve is drawn through the outer critical point which very nearly coincides with the Parker critical point. The dashed line shows the decelerating solutions spiralling into the attractor.

Table 2b shows that the wind velocity at the stellar surface for the low velocity solution for α equal to 500 and λ equal to 2 is remarkably high. This is shown in Fig. 6. The proximity of the attractor to the first critical point affects the accelerating solution through that point. The wind now decelerates over 10 stellar radii before accelerating again. Physically the wind is accelerated by the sound waves, but after these are dissipated the wind decelerates under the influence of gravity until the Parker thermal mechanism accelerates the wind again. In Fig. 6 the high

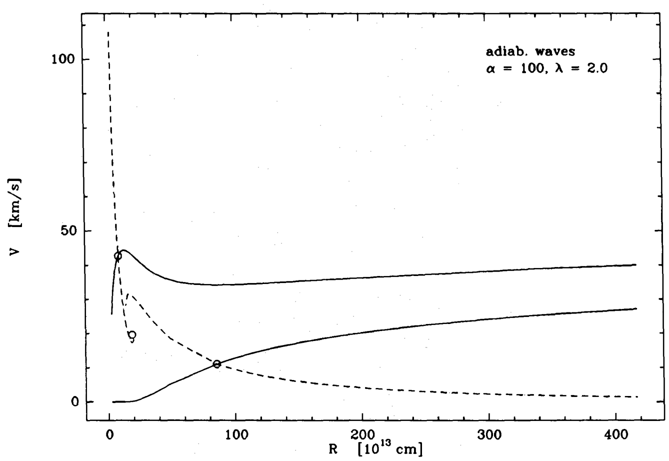

Fig. 5. Velocity profiles for $\alpha = 100$, $\lambda = 2.0$, adiabatic waves. Upper solid curve is high-velocity solution. Lower solid curve is low-velocity solution. Drawn dashed are decelerating solutions spiralling into the attractor represented by a filled circle. Open circles are the first and third critical points

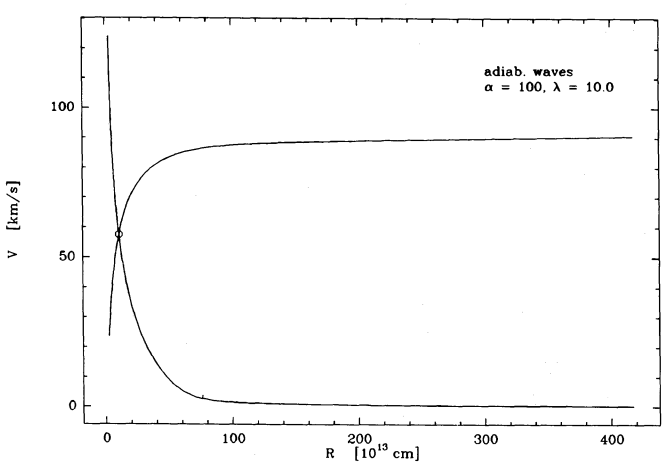

Fig. 4. Velocity profiles; accelerating and decelerating solutions, for $\alpha = 100$, $\lambda = 10$, adiabatic waves

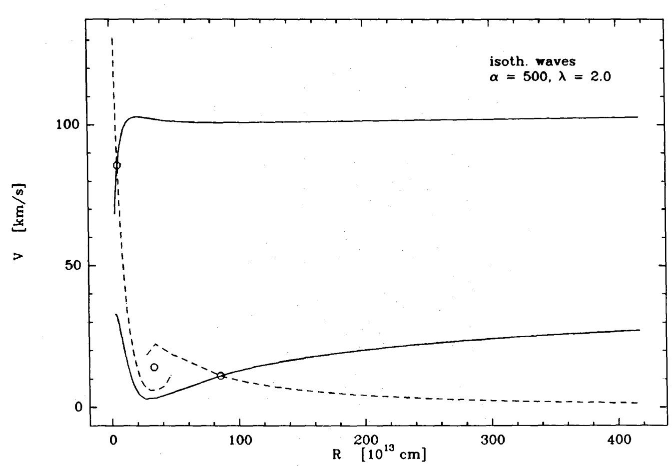

Fig. 6. Velocity profiles for $\alpha = 500$, $\lambda = 2.0$, isothermal waves

velocity solution and the decelerating solutions spiralling into critical point number 2 are also shown. Similar solutions exist for all λ less than the threshold value of approximately 5, both for solutions driven by adiabatic waves and for solutions driven by isothermal waves.

6. Comparison of sound wave driven winds with Alfvén wave driven winds

Table 5 shows some results of adiabatic sound-wave-driven winds calculated with a particle density at the base of the wind of $10^{11}\,\mathrm{cm}^{-3}$. This density and the stellar parameters used (16 solar masses and 400 solar radii) make the results directly comparable with the first six models given by Hartmann and MacGregor (1980). Their results are reproduced in Table 6. The tables show the energy flux of waves at the base of the wind, the resulting mass loss rate and the velocity of the wind at 150 stellar radii. In addition Table 6 shows the Alfvén wave velocity at the stellar surface and at 150 stellar radii.

To produce sound-wave-driven wind models for which the flux of sound waves equals the flux of Alfvén waves in the Hartmann and MacGregor (1980) results would require a considerable amount of work in producing interpolated models, but Tables 5 and 6 do show the differences between the two theories. For waves with no dissipation, a sound wave flux of $2.43\,10^5$ erg $\mathrm{cm}^{-2}\,\mathrm{s}^{-1}$ gives a mass loss rate of $6.02\,10^{-7}\,\mathcal{M}_\odot\,\mathrm{yr}^{-1}$, whereas the Alfvén wave model with a flux of $4.20\,10^5\,\mathrm{erg\,cm}^{-2}\,\mathrm{s}^{-1}$ gives the smaller mass loss rate of $4.32\,10^{-8}\,\mathcal{M}_\odot\,\mathrm{yr}^{-1}$. The big difference is in the velocity of the winds at 150 stellar radii, $508\,\mathrm{km\,s}^{-1}$ for the Alfvén wave driven wind and $89.4\,\mathrm{km\,s}^{-1}$ for the sound wave driven wind. This difference comes from the Alfvén speed being much higher near to the star than the sound speed. The Alfvén speed at the stellar surface and at 150 stellar radii is given for each model in Table 6. The adiabatic sound speed is $14.37\,\mathrm{km\,s}^{-1}$. The Mach numbers in the solutions are comparable.

For waves with a dissipation length of one stellar radius, the wind velocities at 150 stellar radii are comparable, whereas the mass loss driven by sound waves is significantly greater.

In Table 5 the mechanical flux and the mass loss rate increase by 24 orders of magnitude when α increases from 100 to 200 when the dissipation length is 1. This occurs because at an intermediate value of α the critical points number 2 and 3 appear. The mechanical flux for the solution passing through critical point number 3 is $7\,10^7\,\mathrm{erg\,cm}^{-2}\,\mathrm{s}^{-1}$ whereas it is less than $10^{-16}\,\mathrm{erg\,cm}^{-2}\,\mathrm{s}^{-1}$ for the solution through critical point number 1. There are stationary solutions for $\lambda = 1$ with a mechanical flux within that 24 orders of magnitude gap. These solutions are low velocity solutions that resemble the solution plotted in Fig. 6 but with a lower velocity at the stellar surface.

As Holzer et al. (1983) have shown there are difficulties in reconciling the theory of Alfvén-wave-driven winds with the observations of the final wind velocities of late type giants and supergiants, which are typically half the escape velocity from the surface of the star. Although these low final wind velocities can be matched with a dissipation length for the Alfvén waves about equal to one stellar radius, Holzer et al. (1983) have shown that the final wind velocity is very sensitive to the assumed dissipation length which would have to be specified to within a few percent to obtain agreement. To require such a closely defined Alfvén wave dissipation length for a wide range of stars makes the explanation seem improbable. In addition there is no physical mechanism which would explain such a dissipation length.

The sound wave driven winds are slow winds. The final velocity is in most cases less than the escape velocity at the surface of the star, and is insensitive to the assumed dissipation length. It appears then that the sound wave driven winds are good candidates for explaining the winds observed in the late type giants and supergiants.

Table 5. Mechanical flux ($\mathrm{erg\,cm}^{-2}\,\mathrm{s}^{-1}$), mass-loss rate ($\mathcal{M}_\odot\,\mathrm{yr}^{-1}$) and velocity ($\mathrm{km\,s}^{-1}$) for models with adiabatic waves. Assumed particle density at r_0 is $10^{11}\,\mathrm{cm}^{-3}$

α	λ	$F_m(r_0)$	$\dot{\mathcal{M}}$	V_{150}
20	∞	$2.49\,10^{-10}$	$1.55\,10^{-21}$	63.14
50	∞	$2.43\,10^{+5}$	$6.02\,10^{-7}$	89.42
100	∞	$2.20\,10^{+7}$	$3.87\,10^{-5}$	117.2
200	∞	$6.22\,10^{+7}$	$8.37\,10^{-5}$	153.6
50	1	$6.16\,10^{-17}$	$1.53\,10^{-28}$	27.12
100	1	$1.24\,10^{-16}$	$1.55\,10^{-28}$	27.12
200	1[a]	$7.03\,10^{+7}$	$1.27\,10^{-4}$	68.79

[a] This is the high-velocity solution.

7. Conclusions

Sound waves may play an important role in driving mass-loss from all stars experiencing some form of acoustic wave motion at their surface, such as nonradial pulsation. It has been shown

Table 6. the magnetic field (G), mechanical flux ($\mathrm{erg\,cm}^{-2}\,\mathrm{s}^{-1}$), mass-loss rate ($\mathcal{M}_\odot\,\mathrm{yr}^{-1}$), velocity at 150 stellar radii and Alfvén velocity at the stellar surface and at 150 stellar radii ($\mathrm{km\,s}^{-1}$) for the models 1 to 6 of Hartmann and MacGregor (1980)

Model	λ	B_0	$F_0(r_0)$	$\dot{\mathcal{M}}$	V_{150}	A_0	A_{150}
1	∞	1	$3.36\,10^3$	$1.09\,10^{-10}$	822.8	8.452	203.1
2	∞	5	$4.20\,10^5$	$4.32\,10^{-8}$	508.1	42.26	40.08
3	∞	10	$3.36\,10^6$	$5.47\,10^{-7}$	407.8	84.52	20.18
4	1	1	$3.36\,10^3$	$5.83\,10^{-11}$	31.61	8.452	54.43
5	1	5	$4.20\,10^5$	$3.14\,10^{-8}$	47.65	42.26	14.40
6	1	10	$3.36\,10^6$	$4.51\,10^{-7}$	50.97	84.52	7.858

that a slow and massive wind can be formed if the initial mechanical flux of sound waves is large enough. If the initial mechanical flux is small, the parameter α is small, and the resulting solution is very similar to the Parker wind. For a small set of combinations of α and λ there are two coëxisting solutions to the equation of motion that are of interest. For λ less than $\lambda_{\text{crit.}}$ and α large enough, a high-velocity solution yielding a large mass-loss, and a low-velocity solution are obtained. The latter is generally very similar to the Parker wind with a negligible mass-loss. Note however that solutions similar to the low velocity solution plotted in Fig. 6 can yield intermediate mass loss rates. The behaviour as a function of α is highly nonlinear. However, the mass-loss rates behave approximately linearly as a function of the true mechanical flux.

For extended stars the ratio of the escape velocity to the speed of sound, which comes into the equation of motion in the parameter Ψ, is small. This means that the decelerating force is small and little energy is required to drive the wind from the star, which is of course advantageous irrespective of the driving mechanism. Specific to the mechanism of sound wave driven winds is that for a more extended star the acceleration of the gas becomes smaller which implies a relatively flat velocity profile. This means that cool supergiants will favour a slow, dense wind.

To obtain Eq. (6) for the acoustic wave pressure, the waveform has to be specified, as well as the behaviour of the gas within the wave and the manner in which the waves dissipate. These three attributes of a wave cannot generally be chosen independently. For sound waves of small amplitude, a description of the waves in terms of α and λ is sufficient.

The influence of the saw tooth form of a shock wave on the wave pressure can easily be expressed by a constant factor because only the amplitude averaged over a waveperiod is of importance. The dissipational behaviour of a shock wave is very different from linear waves and the waveform of a dissipating shock wave is generally not constant. The gradient of the wave-pressure, which comes into the equation of motion is then a rather more complicated function of r and u, than that used in this paper.

The waves are assumed to be either adiabatic or isothermal. The influence of this on the solutions is small. A more complete description of the gas in this respect does not seem necessary at this point. Similarly, if the waveform and the manner in which the waves dissipate are assumed to be independent, explicit calculation of the wave pressure tensor arising from various waveforms will not yield essentially different results, because the waveform can then be expressed by a constant.

Acknowledgements. F.P. Pijpers acknowledges support by the Netherlands foundation for Astronomical Research (ASTRON), which is financially supported by the Netherlands Organization for the advancement of Pure Research (ZWO). The authors are grateful to Dr P. Ulmschneider for a number of suggestions for improving the presentation of this paper, and to Dr G.H. Bowen for sending a copy of his paper in advance of publication.

Appendix A. The critical points

In the critical points $(\xi, M) = (\xi_c, M_c)$ of Eq. (28), both left- and right-hand sides of (28) are equal to 0. This reduces to the two following conditions:

$$1 + \frac{3b_1 M_c \varepsilon_c}{M_c + 1} - b_0 M_c^2 = 0 \tag{A1}$$

$$\frac{2\Psi}{\xi_c^2} - \frac{2}{\xi_c}(1 + \tfrac{3}{2}b_2\varepsilon_c) - \frac{3b_1\varepsilon_c}{2\lambda} = 0 \tag{A2}$$

The properties of the critical points in general will be discussed, after two limiting cases for the parameters α and λ have been isolated.

– The solution for the critical point in an atmosphere without waves: $\alpha = 0$, and therefore $\varepsilon = 0$.
Equations (A1, A2) are reduced to:

$$\begin{aligned} &1 - b_0 M_c^2 = 0 \\ &\frac{2\Psi}{\xi_c^2} - \frac{2}{\xi_c} = 0 \end{aligned} \tag{A3}$$

r_c and u_c can be substituted back into these equations which yields:

$$\begin{aligned} r_c &= \Psi r_0 = \frac{G\mathcal{M}_* \mu \mathrm{m}}{2kT} \\ u_c &= \frac{a}{\sqrt{b_0}} = \sqrt{\frac{kT}{\mu \mathrm{m}}} \end{aligned} \tag{A4}$$

This critical point is identical to that of the Parker theory.

– The solution for the critical point in an atmosphere where the waves are dissipationless: $\alpha \neq 0$, $\lambda \to \infty$.
Equation (A1) turns into a polynomial of fifth degree in M_c.

$$(M_c + 1)^3(1 - b_0 M_c)^2 + 3b_1\alpha M_c^2 = 0 \tag{A5}$$

which has one solution for M_c greater than zero.
Equation (A2) can be rewritten into an expression for ξ_c in terms of M_c:

$$\xi_c = \Psi \Big/ \left[1 + \frac{3b_2\alpha M_c}{2(M_c + 1)^2}\right] \tag{A6}$$

Since α, Ψ and M_c are all greater than zero, the possible values of ξ_c and M_c as deduced from (A5) and (A6) are:

$$\begin{aligned} &M_c > \frac{1}{\sqrt{b_0}} \\ &\xi_c \leqq \Psi \end{aligned} \tag{A7}$$

Note that for isothermal waves $b_2 = 0$ and therefore $\xi_c = \Psi$ for all α. Since Eq. (19) describes the behaviour of the wave energy-density only for ξ greater than 1, ξ_c has to be greater than 1. Combining this with the above constraints, this model is only valid for Ψ greater than 1. If Eq. (19) is assumed to be valid also for ξ less than one, this restriction can of course be dropped.

In the remainder of this appendix, α can be assumed to be greater than zero, and λ finite. Substituting Eq. (19) into (A1) and rearranging terms is now allowed and yields:

$$\xi_c = 1 - \lambda \log\left[\frac{(M_c + 1)^3(b_0 M_c^2 - 1)}{3b_1\alpha M_c^2}\right] \tag{A8}$$

The term between brackets has to be greater than zero, which again yields the constraint for M_c expressed in Eq. (A7). Multiplying Eq. (A2) by $\frac{1}{2}\xi_c^2$, and substituting (19) yields:

$$(\Psi - \xi_c)(M_c + 1)^2 - \left(\tfrac{3}{2}b_2\alpha + \frac{3b_1\alpha}{4\lambda}\xi_c\right)\tilde{e}M_c = 0 \tag{A9}$$

Here $\tilde{e}$ stands for:

$$\tilde{e} = \xi_c \exp[(1-\xi_c)/\lambda] \tag{A10}$$

For ξ_c equal to Ψ, Eq. (A9) has no physically valid solution. Excluding this case, the solutions of Eq. (A8) can be put into the form:

$$M_c = f - 1 \pm \sqrt{(f^2 - 2f)} \tag{A11}$$

with

$$f = \frac{3}{4}\alpha\left(b_2 + \frac{b_1}{2\lambda}\xi_c\right)\frac{\tilde{e}}{(\Psi - \xi_c)} \tag{A12}$$

From (A11) it can be seen that the solutions separate into three categories for different values of f. For f between 0 and 2, no real solutions for M_c exist, which is physically unacceptable. For f less than zero all solutions for M_c are less than zero, which does not describe a stellar wind, but accretion. Equation (A11) therefore yields a constraint for f. Substituting this constraint in Eq. (A12) will yield a constraint for ξ_c:

$$\tilde{e} \geqq \frac{8(\Psi - \xi_c)}{3\alpha}\left(b_2 + \frac{b_1}{2\lambda}\xi_c\right) \quad \text{for } \xi_c < \Psi \tag{A13a}$$

$$\tilde{e} \leqq \frac{8(\Psi - \xi_c)}{3\alpha}\left(b_2 + \frac{b_1}{2\lambda}\xi_c\right) \quad \text{for } \xi_c > \Psi \tag{A13b}$$

Only (A13a) can be satisfied, since $\tilde{e}$ is greater than zero for all positive ξ_c and the righthand side of (A13b) is less than zero for all ξ_c greater than Ψ. Therefore, ξ_c again has to be less than Ψ.

For given values of α, λ, f and Ψ Eq. (A12) can have as many as three solutions for ξ_c, if λ is less than a certain critical value. This can be seen by rewriting (A12) into:

$$\frac{8\lambda f}{3\alpha b_1}\frac{(\Psi - \xi_c)}{(2\lambda b_2/b_1 + \xi_c)} - \xi_c \exp[(1-\xi_c)/\lambda] \equiv G(\xi_c) = 0 \tag{A14}$$

If there are three solutions of (A14), there are values of ξ_c for which:

$$G'(\xi_c) = 0 \quad \text{and} \quad G(\xi_c) \geqq 0 \tag{A15}$$

Conditions (A15) yield a cubic equation which only has three real solutions if λ satisfies:

$$\lambda < \lambda_{\text{crit.}} = \lambda' \Psi \tag{A16}$$

For isothermal waves λ' equals $3 - 2\sqrt{2}$. λ' is slightly more for adiabatic waves. For λ greater than this value, only one solution for ξ_c of equation (A2) exists. Note that even if λ is less than $\lambda_{\text{crit.}}$, this does not necessarily mean that there are three critical points, but only that curve IIb in Fig. 1 exists. Condition (A14) is necessary but not sufficient for the existence of three critical points because curve IIb in Fig. 1 has to intersect curve I. This only happens for a certain range of values of α for any $\lambda < \lambda_{\text{crit.}}$.

Appendix B. The character of critical points

Equation (27) can symbolically be written as:

$$\frac{dM}{d\xi} = \frac{f(\xi, M)}{g(\xi, M)} \quad \text{or} \quad \begin{pmatrix} d\xi \\ dM \end{pmatrix} = \begin{pmatrix} g \\ f \end{pmatrix} \tag{B1}$$

where

$$f(\xi_c, M_c) = g(\xi_c, M_c) = 0 \tag{B2}$$

Now regard the formal numerical integration as an iterative process:

$$\begin{cases} \xi_{i+1} = \xi_i + g(\xi_i, M_i) \\ M_{i+1} = M_i + f(\xi_i, M_i) \end{cases} \tag{B3}$$

and construct a first order Taylor expansion of this process around the critical point.

$$u_{i+1} = \begin{pmatrix} 1 + \dfrac{\partial g}{\partial \xi} & \dfrac{\partial g}{\partial M} \\ \dfrac{\partial f}{\partial \xi} & 1 + \dfrac{\partial f}{\partial M} \end{pmatrix} u_i \quad \text{with } u_j = \begin{pmatrix} \xi_j - \xi_c \\ M_j - M_c \end{pmatrix} \tag{B4}$$

The eigenvalues and eigenvectors of this matrix can be calculated. If the two eigenvalues are different and real, the two eigenvectors $\tilde{u}$ and $\tilde{v}$ correspond to the solutions of accelerating flow and decelerating flow respectively. Let

$$\tilde{u} = \begin{pmatrix} \tilde{u}_1 \\ \tilde{u}_2 \end{pmatrix} \quad \text{and} \quad \tilde{v} = \begin{pmatrix} \tilde{v}_1 \\ \tilde{v}_2 \end{pmatrix} \tag{B5}$$

be the two eigenvectors, then:

$$\left(\frac{dM}{d\xi}\right)_c = \frac{\tilde{u}_2}{\tilde{u}_1} \quad \text{and} \quad \left(\frac{dM}{d\xi}\right)_c = \frac{\tilde{v}_2}{\tilde{v}_1} \tag{B6}$$

for the accelerating and decelerating solutions respectively.

There is now a coordinate system in which the matrix has the form:

$$A = \begin{pmatrix} e_1 & 0 \\ 0 & e_2 \end{pmatrix} \tag{B7}$$

with $e_{1,2}$ the eigenvalues. Functions of the x and y coordinate in the new system, of the form:

$$y = ax^b \quad \text{with } b = \log e_2 / \log e_1 \text{ and } a \text{ real} \tag{B8}$$

will be invariant under repeated application of the matrix transformation A.

If the eigenvalues are equal, there is only one solution. This is a nodal point. The matrix A will now have the form:

$$A = \begin{pmatrix} e & \dfrac{\partial g}{\partial M} - \dfrac{\partial f}{\partial \xi} \\ 0 & e \end{pmatrix} \tag{B9}$$

with e the eigenvalue. Invariant curves are now of the form:

$$x = by\frac{\log(y/y_0)}{\log e} \quad \text{with } b = \left(\frac{\partial g}{\partial M} - \frac{\partial f}{\partial \xi}\right)\Big/ e \text{ and } y_0 \text{ real} \tag{B10}$$

If the eigenvalues have imaginary parts for a given critical point, no continuously differentiable velocity curve passing through that point can be constructed. Define eigenvalues λ, and eigenvectors v:

$$\lambda, \bar{\lambda} = \rho e^{\pm i\phi} \quad v, \bar{v} = v_1 + iv_2 \quad \text{with } \rho, \phi, v_1 \text{ and } v_2 \text{ real} \tag{B11}$$

and express all u in terms of v_1 and v_2; $u_i = a_i v_1 + b_i v_2$. The expression for u_{i+1} is then:

$$u_{i+1} = \rho[(a_i v_1 + b_i v_2)\cos\phi + (b_i v_1 - a_i v_2)\sin\phi] \tag{B12}$$

This describes a step along a spiral path around the critical point. Such a critical point is an attractor for all $\rho \neq 1$. The structure of solutions around all types of critical points is described in more detail in a paper by Holzer (1977).

References

Abramowitz, M., Stegun, I.A.: 1970, "Handbook of mathematical functions", Dover publications, p. 13

Bretherton, F.P.: 1970, Lect. in Appl. Math. (Am. Math. Soc.) **13**, 61

Bowen, G.H.: 1988, *Astrophys. J.* (in press)

Castor, J.I.: 1987, "Instabilities in luminous early type stars", eds. H.J.G.L.M. Lamers and C.W.H. de Loore, Reidel, p. 159

Hall, G., Watt, J.M., eds.: 1976, Modern numerical methods for ordinary differential equations, Clarendon press.

Hartmann, L., MacGregor, K.B.: 1980, *Astrophys. J.* **242**, 260

Holzer, T.E., Flå, T., Leer, E.: 1983, *Astrophys. J.* **275**, 808

Holzer, T.E.: 1977, *J. of Geophys. Res.* **82**, 23

Jacques, S.A.: 1977, *Astrophys. J.* **215**, 942

Kwok, S.: 1975, *Astrophys. J.* **198**, 583

Landau, L.D., Lifshitz, E.M.: 1959, "Fluid mechanics", Pergamon press, p. 12, p. 256

Linsky, J.L., Haisch, B.M.: 1979, *Astrophys. J.* **229**, 427

Parker, E.N.: 1958, *Astrophys. J.* **128**, 664

Willson, L.A., Hill, S.J.: 1979, *Astrophys. J.* **228**, 854

Wood, P.R.: 1979, *Astrophys. J.* **227**, 220